Incorporation of Spiroxanthene Units in Blue-Emitting Oligophenylene Frameworks: A New Molecular Design for OLED Applications

ARTICLE *in* CHEMISTRY - A EUROPEAN JOURNAL · NOVEMBER 2011

Impact Factor: 5.73 · DOI: 10.1002/chem.201100790 · Source: PubMed

5 AUTHORS, INCLUDING:

Cyril Poriel
Université de Rennes 1
73 PUBLICATIONS **1,005** CITATIONS
SEE PROFILE

Joëlle Rault-Berthelot
Université de Rennes 1
106 PUBLICATIONS **1,707** CITATIONS
SEE PROFILE

DOI: 10.1002/chem.201100790

Incorporation of Spiroxanthene Units in Blue-Emitting Oligophenylene Frameworks: A New Molecular Design for OLED Applications

Cyril Poriel,*[a] Nicolas Cocherel,[a] Joëlle Rault-Berthelot,[a] Laurence Vignau,[b] and Olivier Jeannin[a]

Abstract: We report herein the incorporation of xanthenyl units into two extended π-conjugated phenylene systems, namely indenofluorene and pentaphenylene. Thus, dispiroxanthene-indenofluorene (DSX-IF) and dispiroxanthene-ladderpentaphenylene (DSX-LPP) have been designed and synthesized through short and efficient synthetic approaches. These two molecules possess a 3π-2-spiro architecture (3π-systems/2-spiro bridges), in which two xanthenyl cores are spirolinked to a π-conjugated backbone either indenofluorene for DSX-IF or pentaphenylene for DSX-LPP. The structural, electrochemical, and photophysical properties of these blue/violet emitters have been studied in detail and compared to those of their 'all carbon' analogues with spirofluorenyl cores instead of spiroxanthenyl cores, namely dispirofluorene-indenofluorene (DSF-IF) and dispirofluorene-ladderpentaphenylene (DSF-LPP), previously reported in the literature. Finally, the application of DSX-IF and DSX-LPP as new light-emitting materials in nondoped organic light emitting diodes is reported. A detailed optical study of the different electroluminescence spectra is notably presented, with an emphasis 1) on the origin of the low-energy emission band observed in the case of DSX-LPP and 2) on the unexpected optical contribution of the well-known hole-transporting-layer NPB (*N*,*N*′-di(naphtyl)-*N*,*N*′-diphenyl(1,1′-biphenyl)-4,4′-diamine).

Keywords: indenofluoroene · low-energy emission bands · OLEDs · organic electronics · pentaphenylene · spiro compounds · xanthene derivatives

Introduction

During the last two decades, organic electronics have attracted considerable interest[1,2] and organic light emitting diodes (OLEDs) appear to be the near future of display applications.[3,4] As the lifetime of blue OLEDs[5] is still shorter than that of the green and red OLEDs, numerous research groups have been involved in the design and synthesis of novel small molecules,[6–30] with stable blue fluorescence emission. One appealing strategy to obtain stable fluorescence in the solid state is to introduce within the oligomer or the polymer backbone a spiro centre.[31,32] This approach called the "spiro concept", in which a common sp^3-hybridized carbon atom links two orthogonal π-conjugated arms has allowed outstanding breakthroughs in the field.[31] Indeed, the spiro concept possesses several advantages, such as suppressing excimer formation in the solid state, improving the thermal and morphological stabilities, increasing the solubility etc..[31] Since the first example of blue electroluminescence based on a spiro derivative,[33] numerous oligomers[12,17,18,31,32,34–41] incorporating spiro bridges have been designed for blue OLED applications. Typically, the core of most of spiro compounds is based on the known 9,9′-spirobifluorene.[31] Recently, new synthetic approaches have been developed to obtain spiro compounds incorporating heteroatoms to tune the optical, electrochemical, or charge-transport properties of the materials.[18,42–46] For example, Salbeck and co-workers have notably reported the first spiro-type derivative constituted of four thiophene units, presenting very appealing charge-transport properties.[47] However, incorporation of spiro centers in xanthene-based materials for organic electronics is almost absent from the literature. One of the simplest spiro-configured xanthene parents is spiro-(fluorene-9,9′-xanthene) SFX, made of a fluorene unit spirolinked to a xanthene core (Scheme 1). The use of the SFX backbone as an emissive layer in blue OLEDs either incorporated in polymers[48–50] or in oligomers[6,51,52] has only been very recently investigated and is still very rare. For example, Huang and co-workers have notably reported for OLED applications, new blue light emitters based on the SFX scaffold.[6,51] Similarly, a SFX-based emitter incorporating oligophenylene units has been recently investigated as an emissive layer within an OLED. This device exhibits a sky-blue emission with a maximum brightness of 1507 $Cd\,m^{-2}$ and a current efficiency of 0.36 $Cd\,A^{-1}$.[52] Despite these very

[a] Dr. C. Poriel, Dr. N. Cocherel, Dr. J. Rault-Berthelot, Dr. O. Jeannin
Université de Rennes 1-UMR CNRS 6226
"Sciences Chimiques de Rennes"-MaCSE group. Bat 10C
Campus de Beaulieu - 35042 Rennes cedex (France)
E-mail: cyril.poriel@univ-rennes1.fr

[b] Dr. L. Vignau
Université de Bordeaux - IMS/UMR CNRS 5218-site ENSCBP
16 Avenue Pey-Berland - 33607 Pessac cedex (France)

Supporting information for this article is available on the WWW under http://dx.doi.org/10.1002/chem.201100790.

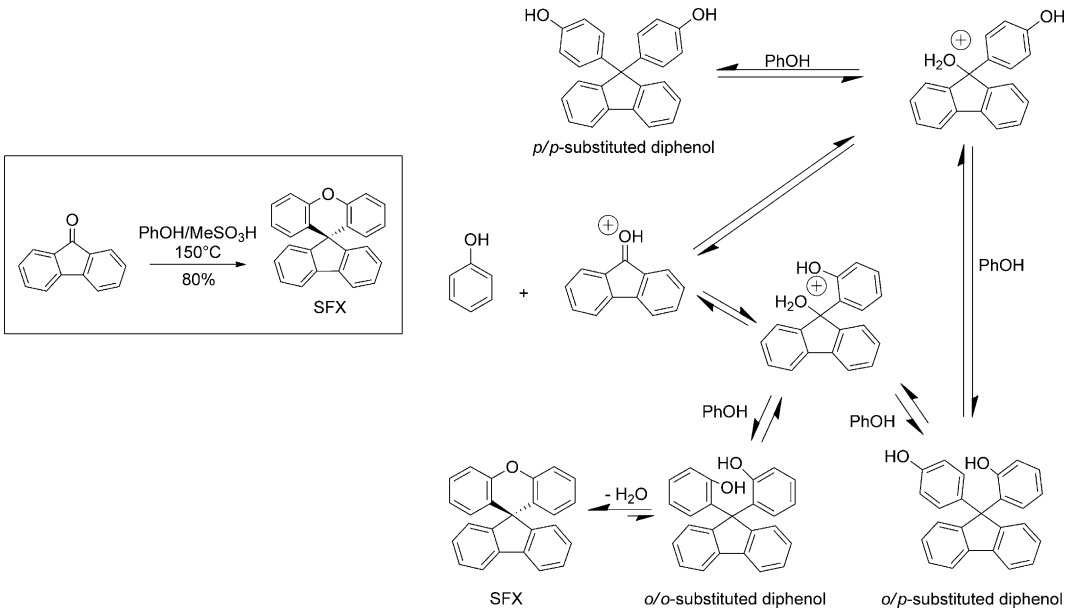

Scheme 1. Synthesis of SFX and plausible mechanism proposed.[75]

recent examples, xanthene-based oligomers have been very weakly studied for organic electronic applications due to the lack of efficient synthetic approaches and SFX is the only example reported to date. To expand the scope of applications of spiro derivatives for electronics, it is hence of great interest 1) to introduce xanthene units into various extended π-conjugated phenylene systems, such as indenofluorene and pentaphenylene, and 2) to develop efficient synthetic methodologies towards these spiro-configured xanthene derivatives.

As our group is strongly involved for many years in the design of spiro-configured materials for blue OLED applications,[53,54] we report herein, promising new blue spiroxanthene emitters based on an indenofluorene framework, namely dispiroxanthene-indenofluorene (DSX-IF), and based on a pentaphenylene framework, namely dispiroxanthene-ladderpentaphenylene (DSX-LPP). These molecules possess a 3π-2-spiro architecture (3π-systems/2-spiro bridges),[54] in which two xanthenyl cores are spirolinked to a π-conjugated backbone either indenofluorene for DSX-IF or pentaphenylene for DSX-LPP. As indenofluorene[3,53,55–65] or pentaphenylene[54,55,66–74] derivatives are highly appealing cores for organic electronics, it is of great interest to investigate the effect of the incorporation of xanthenyl units in such frameworks. In this work, as a development to our preliminary note,[56] we first report our investigations towards the synthesis of DSX-IF and DSX-LPP through different, efficient, and short synthetic approaches. The structural, electrochemical, thermal, and photophysical properties of these blue/violet emitters will be discussed, together with their first application as an emissive layer in small molecule OLED (SMOLED). Finally, a detailed optical study of the different electroluminescence spectra is presented, with an emphasis 1) on the origin of the low-energy emission band observed in the case of DSX-LPP and 2) on the unexpected optical contribution of the well-known hole-transporting-layer NPB (*N*,*N*′-di(naphtyl)-*N*,*N*′-diphenyl(1,1′-biphenyl)-4,4′-diamine). This work constitutes, to the best of our knowledge, the first incorporation of xanthene units within indenofluorene and pentaphenylene frameworks and one of the rare examples of nondoped SMOLEDs based on xanthene derivatives.

Results and Discussion

Synthesis: Due to the lack of efficient and convenient synthetic approaches, xanthene derivatives and especially spiroxanthene derivatives have been very rarely studied for organic electronics applications. As the synthesis of new materials is strongly sought worldwide for organic electronics applications it is crucial to develop efficient routes towards novel fluorophores, such as spiroxanthene derivatives, to fully explore their potential. For example, Huang and coworkers have reported an elegant but unexpected one-pot synthesis of SFX (Scheme 1) from a mixture of 9-fluorenone, phenol, and $MeSO_3H$, involving a thermodynamically controlled cyclization reaction as the key step.[75] Thus, they have hence postulated that the thermodynamic-controlled product of the reaction is SFX and that the kinetic-controlled product of the reaction is a *para*/*para*-substituted diphenol derivative (Scheme 1).

In the light of these results, we decided to follow the same strategy to introduce the xanthenyl units within the pentaphenylene core (DSX-LPP) and within the indenofluorenyl core (DSX-IF). In this context, the corresponding diketones, pentaphenylenedione **1**[53] and indenofluorenone **3**[54] were the key intermediates (Schemes 2 and 3).

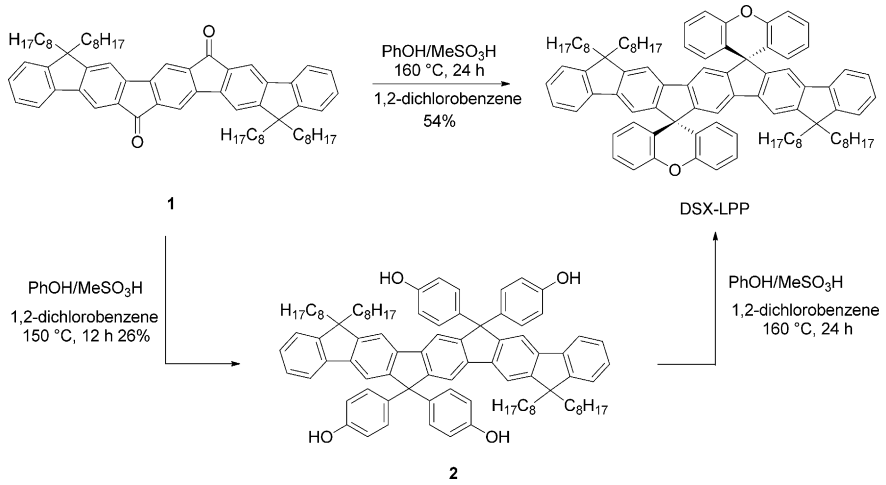

Scheme 2. Synthesis of DSX-LPP and tetraphenol derivative **2**.

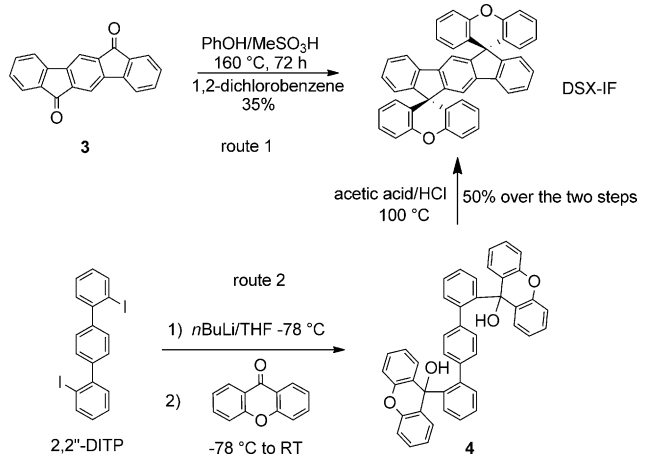

Scheme 3. Synthesis of DSX-IF: Routes 1 and 2.

Thus, DSX-LPP was synthesized from a mixture of diketone **1**,[54] $MeSO_3H$, and phenol (54% yield; Scheme 2). By decreasing the reaction time, the tetraphenol derivative **2**, with 4-*para*-hydroxyphenyl units, was isolated and further cyclized into DSX-LPP under the same experimental conditions. Tetraphenol **2** appears hence as the kinetic-controlled product and DSX-LPP as the thermodynamic-controlled product. These results are in accordance with the mechanism postulated for the synthesis of SFX (Scheme 1).

Similarly DSX-IF was also obtained in a one-pot approach with 35% yield, from a mixture of diketone **3**,[53] $MeSO_3H$, and phenol (Scheme 3, route 1). In contrast to the synthetic approach of DSX-LPP presented above (Scheme 2), we did not manage to isolate the indenofluorene-tetraphenol derivative, analogue of **2**, maybe due to the very low solubility of the indenofluorene derivatives. Indeed, diketone **3** and DSX-IF appear to be poorly soluble in common organic solvents. This very low solubility of the starting diketone **3** is also surely responsible for the moderate yield of the reaction (35%). Owing to the importance of indenofluorene[3,53,55–65] or pentaphenylene[54,55,66–74] derivatives in organic electronics, this approach offers a simple, easy to perform, and highly adaptable access to various π-conjugated building blocks bridged by spiroxanthenyl units.

Despite the fact that this approach offered a rapid access to DSX-IF, the yield of the reaction was, however, too low for future optoelectronic applications and we thus decided to revisit the synthetic approach. The idea was to first introduce the xanthenyl units prior to the formation of the indenofluorenyl core. This new approach is based on a coupling reaction between the known 2,2"-diodinated terphenyl (2,2"-DITP)[53] and a ketone derivative with the xanthenyl core already in place, namely xanthone (Scheme 3, route 2). Thus, the lithium–iodine exchange of 2,2"-DITP with *n*-butyllithium followed by the addition of commercially available xanthone afforded the dixanthenol **4**, which was immediately involved in an intramolecular cyclization reaction giving in fine DSX-IF with a 50% yield over the two steps. Although route 2 has an extra step compared with route 1, none of the steps requires the use of column chromatography for both the purification of dixanthenol **4** and DSX-IF and the overall yield is higher than the one-step approach.

It should be stressed that the ^{1}H NMR spectra of DSX-LPP and DSX-IF are very similar to those of their 'all carbon' analogues with spirofluorenyl cores instead of spiroxanthenyl cores, namely dispirofluorene-indenofluorene (DSF-IF)[53] and dispirofluorene-ladderpentaphenylene (DSF-LPP)[54] previously reported. We note, however, in the ^{1}H NMR spectra of DSX-LPP and DSX-IF, two sets of shielded hydrogen atoms, $\delta = 6.85/6.55$ ppm for DSX-LPP and $\delta = 6.79/6.45$ ppm for DSX-IF (see spectra in the Supporting Information). These signals are not present in the ^{1}H NMR spectra of DSF-LPP and DSF-IF and correspond to the hydrogen atoms of the xanthenyl units in the α- and β-position of the C–O linkage. This shielding effect is due to the electro-donating behavior of the intracyclic oxygen atom. In ^{13}C NMR spectra, the oxygen atom also leads to a strong shielding of the spiro carbon chemical shift, recorded around $\delta = 54$ ppm instead of the ordinary chemical shift of $\delta = 66$ ppm, observed for most of the spiro compounds.[54]

Physicochemical properties of spiroxanthene derivatives

Structural properties: The poor solubility of DSX-IF does not allow us to obtain a suitable single crystal. However, single crystals of DSX-LPP were obtained by liquid–liquid

diffusion of MeOH into a solution of $CDCl_3$ and analyzed by X-ray diffraction to elucidate its molecular structure and packing characteristics. DSX-LPP crystallizes with one molecule of $CDCl_3$, in the triclinic system, space group $P\bar{1}$, with the DSX-LPP unit on an inversion center and a $CDCl_3$ molecule in general position.

DSX-LPP presents a linear antarafacial geometry[76] and its pentaphenylene core (19.4 Å long) does not adopt a strict coplanar configuration as two distorsions are observed on both sides (Figure 1). The dihedral angles between the

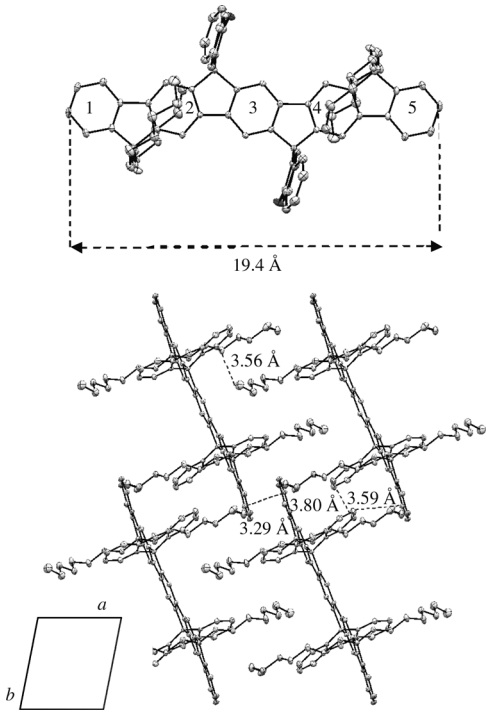

Figure 1. Molecular structure (top) and crystal packing diagram along the *c* stacking axis (bottom) of DSX-LPP obtained from single-crystal X-ray diffraction data. The hydrogen atoms have been omitted for clarity.

plane of the central phenyl ring 3 and those of side rings 1 and 5 are of approximately 7° (see phenyl rings labeling in Figure 1, top). These distortions are comparable to those observed for a similar derivative with fluorenyl units instead of xanthenyl (8.4°).[54] The xanthenyl cores do not add, hence any significant structural deformations of the central pentaphenylene compared to the fluorene units. The angles between the plane of the central phenyl ring 3 of the pentaphenylene and those of the phenyl rings of the xanthenyl units are recorded around 81.3 and 80.3° (see the Supporting Information). Indeed, the phenyl rings of the xanthenyl cores of DSX-LPP are not planar as a dihedral angle of 18.2° is observed between the planes of each phenyl ring. This dihedral angle is larger than that observed for SFX.[48]

As indicated in the crystal packing diagram of DSX-LPP (Figure 1, bottom), the closest C–C distance, between two xanthenyl moieties of two neighboring molecules was estimated to be 3.8 Å, greater than the sum of the van der Waals radii of two carbon atoms. Oppositely, the closest C–C distance between two terminal phenyl rings of the pentaphenylene moieties of two neighboring molecules was estimated to be 3.29 Å. This short C–C distance is also observed between the same carbon atoms in the case of its "all carbon" analogue DSF-LPP with spirofluorene units instead of spiroxanthene,[54] suggesting that the arrangement of the pentaphenylene cores is not strongly influenced by the spirolinked π-systems (fluorene or xanthene). These intermolecular C–C distances are smaller than the sum of the Van Der Waals radii of two sp^2 carbon atoms and leads us to conclude that intermolecular interactions may occur, which can lead to parasite bands in fluorescence spectroscopy (see the optical section below). We also note a rather short C–C distance between methylene carbon atoms of the alkyls chains (ca 3.56 Å) and between the xanthene moieties and the pentaphenylene moieties (ca 3.59 Å; Figure 1, bottom).

Electrochemical properties: The redox properties of DSX-IF and DSX-LPP were investigated by cyclic voltammetry (CV) and compared to their 'all carbon' congeners DSF-IF and DSF-LPP (Figure 2).[53,54] DSX-LPP presents in CV two

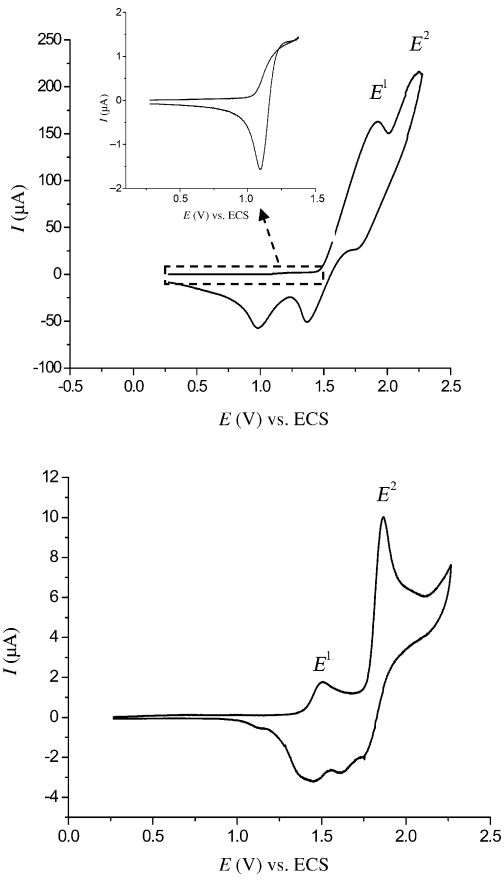

Figure 2. Cyclic voltammetry of DSX-LPP (top, inset: the 0/1.4 V portion) and of DSX-IF (bottom) (2×10^{-3} M in CH_2Cl_2 (Bu_4NPF_6, 0.2 M); working electrode: Pt disk diameter = 1 mm; sweep rate = 100 mV s^{-1}).

irreversible oxidation waves with maxima recorded at $E^1 = 1.92$ and $E^2 = 2.25$ V versus SCE (Figure 2, top). This behavior appears to be very different to that observed for its congener DSF-LPP,[54] both in terms of intensity of the oxidation waves and in terms of potential values. Indeed, for similar concentrations, the first oxidation wave of DSX-LPP (1.92 V; Table 1) has an intensity greater than 150 μA, whereas the first oxidation wave of DSF-LPP (1.09 V) has an intensity lower than 2 μA. This observation leads us to focus DSX-LPP CV studies on the 0.2/1.4 V potential range (see inset in Figure 2, top). In this portion, one can observe a "quasi-reversible" wave, with an intensity of 1.5 μA in accordance with the first oxidation wave of DSF-LPP.[54] As the onset potential of this wave is recorded around 1.05 V, almost identical to that of DSF-LPP (0.96 V),[54] it is then reasonable to contend that the first oxidation of DSX-LPP occurs on the pentaphenylene central core.

Table 1. Electrochemical data for DSF-IF, DSX-IF, DSF-LPP, and DSX-LPP (vs. SCE).

	E^1	E^2	E^{ox}_{onset}	E^{red}_{onset}	HOMO[a]	LUMO[b]	LUMO[c]	ΔE^{el}[d]	ΔE^{opt}[e]
DSX-IF	1.5	1.86	1.39	−2.25	−5.79	−2.15	−2.23	3.64	3.53
DSF-IF[78]	1.47	1.95	1.36	−2.23	−5.76	−2.17	−2.25	3.59	3.51
DSX-LPP	–[f]	1.92	1.05[g]	−2.2	−5.45	−2.2	−2.36	3.25	3.09
DSF-LPP[54]	1.09	1.66	0.96	−2.3	−5.36	−2.1	−2.29	3.26	3.07

[a] Calculated from the onset oxidation potential E^{ox}_{onset}. [b] Calculated from the onset reduction potential E^{red}_{onset}. [c] Calculated from the HOMO energy level (obtained from redox data) and the edge of optical gap. [d] $\Delta E^{el} = |\text{HOMO–LUMO}|$ from redox data. [e] Calculated from the edge of the absorption spectrum in solution by using $\Delta E^{opt} = hc/\lambda$ (ΔE^{opt} (eV) = 1237.5/λ (nm)). [f] A low-intensity wave is recorded around 1.1 V with no clear maximum. [g] From the low-intensity wave at 1.1 V.

Contrary to DSX-LPP discussed above, DSX-IF oxidation occurs along two processes with maxima recorded at $E^1 = 1.5$ and $E^2 = 1.86$ V (Figure 2, bottom), almost identical to those reported for its 'all carbon' congener DSF-IF (1.47 and 1.95 V).[53] Hence, the first oxidation of DSX-IF, as already observed for DSF-IF, involves the indenofluorenyl core in a one-electron process, whereas the second oxidation occurs on the two spirolinked xanthenyl units. The first oxidation peak of DSX-IF ($E^1 = 1.5$ V) is, however, shifted compared with that of the indenofluorene molecule ($E^1 = 1.31$ V),[53] resulting from the electron-withdrawing effect of the spirolinked xanthenes.

DSX-IF and DSX-LPP reductions were studied in the cathodic range and were both observed close to the dichloromethane electrolyte discharge (see the Supporting Information). The shift of the discharge, however, allowed the determination of the onset reduction potentials of DSX-IF (−2.25 V) and DSX-LPP at (−2.2 V).

The gaps obtained from electrochemical data of DSX-IF, $\Delta E^{el} = 3.64$ eV, and DSX-LPP, $\Delta E^{el} = 3.25$ eV, are wide and are consistent with the measured optical gaps ΔE^{opt} with, however, a small deviation (0.15 eV or less). Thus, DSX-LPP presents an electrochemical gap contracted by approximately 0.4 eV compared with that of DSX-IF. The estimated HOMO and LUMO[1] energy levels (obtained from electrochemical data and by using an SCE energy level of 4.4 V relative to vacuum)[77] were: HOMO: −5.45 eV and LUMO: −2.2 eV for DSX-LPP and HOMO: −5.79 eV and LUMO: −2.15 eV for DSX-IF. Thus, DSX-LPP possesses a HOMO level lying 0.34 eV higher than that of DSX-IF due to the extension of the π-conjugation of the central core. Oppositely, the LUMO levels of DSX-IF and DSX-LPP are very similar and do not seem to be influenced by the extension of the π-conjugation of the central core.

Compared to their 'all carbon' analogues DSF-IF and DSF-LPP,[53,54] DSX-IF and DSX-LPP present very similar gaps and energy levels clearly signing that the main properties of these systems are driven by their corresponding central cores (indenofluorene and pentaphenylene). However, the HOMO levels of DSX-IF and DSX-LPP present a slight stabilization compared to those of DSF-IF and DSF-LPP (Table 1). This stabilization is due to the presence of the xanthenyl units, which hence allow a fine-tuning of the HOMO/LUMO energy levels of these systems.

Optical properties: UV/Vis absorption spectrum of DSX-LPP in solution presents a well-defined vibronic structure with $\lambda_{max} = 391$ nm (Figure 4, top). Similarly, DSX-IF also possesses a well-defined spectrum ($\lambda_{max} = 344$ nm, Figure 3, top) but hypsochromically shifted by 47 nm ($\Delta E^{opt} = 3.09$ eV for DSX-LPP vs. 3.53 eV for DSX-IF; vide supra), clearly signing the extension of the conjugation of the central π-system.

The fluorescence maxima of DSX-LPP recorded at 395 and 419 nm (Figure 4, bottom) appear also to be redshifted compared to those of DSX-IF, that is, 347 and 364 nm (Figure 3, bottom). These two first transitions have been assigned to the 0–0 and 0–1 singlet transitions as already observed for similar compounds.[79] The fluorescence quantum yield in solution is very high (91% for DSX-LPP vs. 63% for DSX-IF; Table 2), indicating that nonradiative decay pathways are nearly suppressed in such structures. These two molecules are hence very efficient violet (DSX-IF) and blue (DSX-LPP) emitters. The Stokes shift[80] of both DSX-LPP and DSX-IF is very small (4 and 3 nm, respectively) and consistent with highly rigid structures with only very

[1] The LUMO energy levels of DSX-LPP and DSX-IF have been obtained not from a clear potential peak but from the intersection of the tangent of the current line with the potential axis and hence these values may contain a non-negligible experimental error (see CV in the Supporting Information). Thus, the LUMO energy levels obtained from the onset reduction potential E^{red}_{onset} and those obtained from optical data, appear to be slightly different (Table 1).

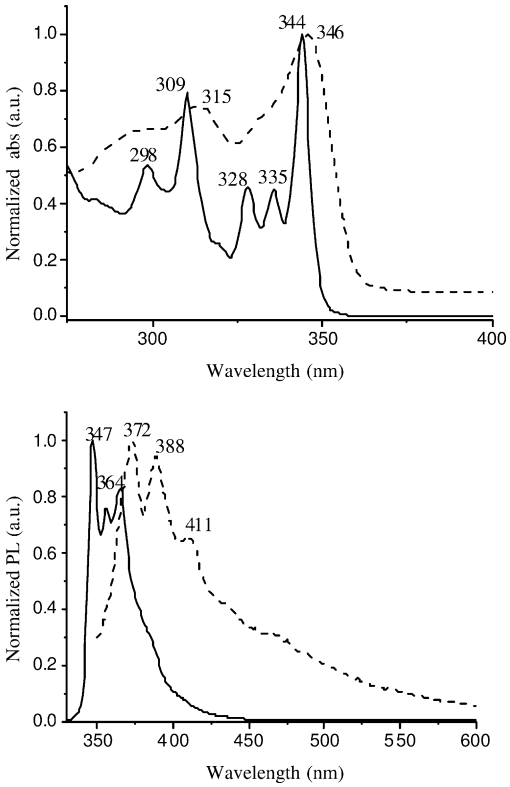

Figure 3. Normalized absorption (top) and fluorescence (bottom, λ_{exc} = 275 nm) of DSX-IF in solution in cyclohexane (8×10^{-7} M, ——) and in spin-coated thin film (10 mg mL^{-1} in pyridine, -----).

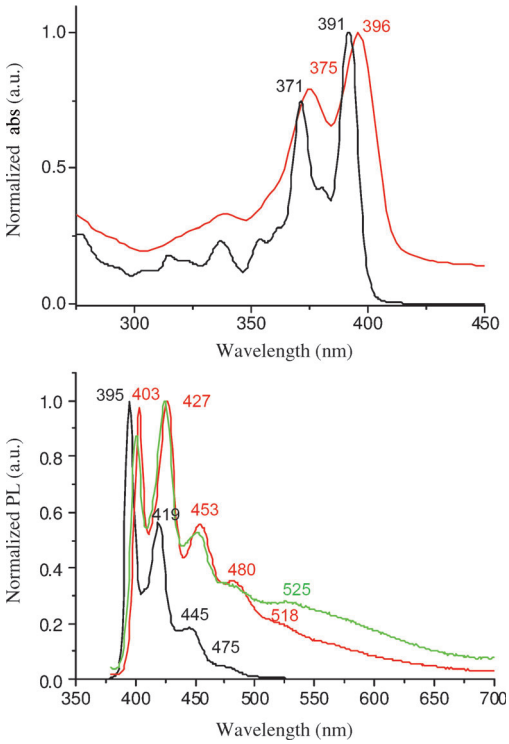

Figure 4. Normalized absorption (top) and fluorescence (bottom, λ_{exc} = 320 nm) of DSX-LPP in solution in cyclohexane (8×10^{-7} M, ——) and in the thin film: spin-coated: 20 mg mL^{-1} from toluene (——); vacuum-deposited (——).

little deformations in the excited state. The thin-film absorption spectrum of DSX-IF (Figure 3, top) is broader than its solution spectrum with only a slight bathochromic shift (2 nm) assigned to the difference between the dielectric constant around the molecules.[81,82] Similarly, a comparison of solution and thin-film fluorescence spectra of DSX-IF also reveals a broader spectrum with a 25 nm redshift between the two first emission peaks (Figure 3, bottom).

The thin-film UV/Vis and fluorescence spectra of DSX-LPP present a fine vibronic structure and are almost identical to their solution spectra, being redshifted only by approximately 5 and 7 nm, respectively (Figure 4), due to the different dielectric constants.[81,82] We also noted a marked difference between solution and thin-film fluorescence spectra of DSX-LPP in the relative intensity of the emission bands, the second fluorescence band at 427 nm being much more intense than the first at 403 nm (Figure 4, bottom). This might be ascribed to self-absorption phenomena due to the overlap of the 0–0 transition emission band and the absorption band that leads to a relative decrease of the intensity of the 0–0 transition.[79,83] This partial self-absorption of the first emission band is due to the very small Stokes shift observed for DSX-LPP.

An important feature, in the case of DSX-LPP, is nevertheless related to the difference observed in the fluorescence spectra, depending of the deposition process (spin-coated vs. vacuum-evaporated; Figure 4, bottom). Indeed, a vacuum-evaporated thin-film of DSX-LPP reveals the presence of a small broad band at low energy (around 525 nm), whereas a spin-coated thin-film does not. Such a difference between the two fluorescence spectra, depending of the deposition process, may be assigned to π–π interchromophore interactions of the pentaphenylene unit. Indeed, the packing arrangement of DSX-LPP (Figure 1, bottom) has revealed some short distances that can be responsible for such optical

Table 2. Optical data and decomposition temperatures T_d.

	λ_{abs}[a] liq. [nm]	λ_{em}[a] liq. [nm]	λ_{abs} solid [nm]	λ_{em} solid [nm]	$\Phi_{soln.}$[d] [%]	T_d[e] [°C]
DSX-LPP	338 (2.70), 371 (3.27), 391 (3.46)	395, 419, 445, 475	338, 375, 396[b]	403, 427, 453, 480[b]	91	397
DSX-IF	298 (2.03), 309 (2.13), 328 (2.08), 335 (2.08), 344 (2.40)	347, 355, 364	315, 346[c]	372, 388, 411 (sh)[c]	63	380

[a] In cyclohexane (8.10^{-7} M) with log ε between brackets. [b] Spin-coated thin film (20 mg mL^{-1} in toluene) [c] Spin-coated thin film (10 mg mL^{-1} in pyridine). [d] The relative quantum yield was measured with reference to quinine sulfate in 1 N H_2SO_4 (Φ = 0.546). The values are estimated ±10%.[61] [e] Decomposition temperatures T_d corresponding to 5% loss have been determined by thermogravimetric analysis (under N_2 atmosphere, rate: 5 °C min^{-1}).

phenomena. This will be discussed in detail below in the OLED section. Such phenomenon was not observed in the case of DSX-IF.

Before any OLED application, the stability of the DSX-IF and DSX-LPP fluorescence spectra as a function of the temperature must be carefully studied.

Gradual heating of the DSX-IF films in air from room temperature to 200 °C (1 h for each stage) does not lead to any modification of the UV/Vis absorption spectrum neither in shape, wavelength, nor in intensity (see the Supporting Information). For DSX-LPP, the behavior is almost identical with nevertheless a decrease in intensity (see the Supporting Information). However, no shift to higher wavelengths, usually linked to strong π–π interchromophore interactions due to aggregation in the solid state, is observed for both compounds.[84]

Gradual heating of a spin-coated thin-film of DSX-IF in air from room temperature to 200 °C (1 h for each stage) does not lead to clear photoluminescent spectral changes (Figure 5, top) and DSX-IF presents hence a high color stability in the solid state.[56] DSX-LPP displays a drastically different behavior as a broad band with two maxima at 493 and 523 nm appears and gradually increases upon heating in ambient atmosphere (Figure 5, bottom). The origin of such contributions at low energy has been extensively studied for the last decade as it remains one important problem in blue OLED technology.[55,85] Indeed, the appearance of the well-known low-energy emission band (also called g-band) has been the subject of debate about its origin.[85] If this low-energy emission band was initially explained by the excimer emission (the formation of dimerized units in the excited state that emit at lower energies) due to the π–π interchromophore interactions of the main π-system,[86] it seems to be agreed nowadays that the low-energy emission band is usually linked to the presence of keto-defects appearing in phenylene derivatives.[87,88]

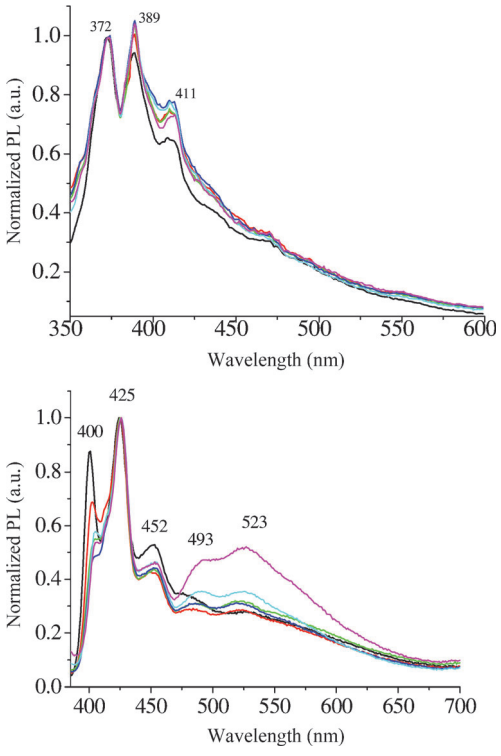

Figure 5. Fluorescence spectra after annealing of top) DSX-IF (spin-coated from pyridine at 10 mg mL^{-1}, λ_{exc} = 275 nm, normalized at 373 nm) and bottom) DSX-LPP (vacuum-deposited, λ_{exc} = 320 nm, normalized at 425 nm) in air at different temperatures (——: after preparation, ——: 1 h at 100 °C, ——: 1 h at 130 °C, ——: 1 h at 160 °C, ——: 1 h at 200 °C, ——: 24 h at 200 °C).

Despite being still debated, one possible manner to determine whether this low-energy emission band arises from keto-defects or excimer emission due to π–π interchromophore interactions of the main π-system is to study the behavior of a DSX-LPP thin-film in the strict absence of oxygen. Indeed, several groups have proposed degradation mechanisms involving atmospheric oxygen as an explanation for the formation of these keto-defects.[88,89] Thus, a spin-coating thin-film of DSX-LPP has been annealed at 200 °C for 24 h under an argon atmosphere and no low-energy band was detected in the corresponding fluorescence spectrum (Figure 6, ——). Then, the film was exposed to ambient atmosphere and heating for a further 24 h. The appearance of a broad low-energy emission band between 480 and 650 nm with two maxima recorded at approximately 493 and 523 nm was clearly evidenced (Figure 6, ——), which indicated that atmospheric oxygen has a strong influence on the appearance of this band. These experiments, in the light of other similar reports,[55,66,69,70,88] support the fact that this low-energy emission band mainly arises from keto-defects formation due to the oxidation of dialkyl bridgeheads and not from aggregation leading to excimer emission of the pentaphenylene units.[2] However, as exposed above, the fluorescence spectrum of a DSX-LPP thin-film at room temper-

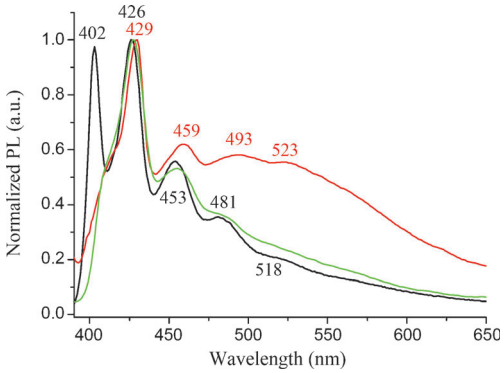

Figure 6. Normalized (425 nm) thin-film fluorescence spectra of DSX-LPP (spin-coated: 20 mg mL^{-1} in toluene, λ_{exc} = 320 nm) at room temperature (——), after annealing under argon (——, 24 h at 200 °C) and after annealing in air (——, 24 h at 200 °C).

[2] It should be noted that when a degraded film of DSX-LPP was redissolved after thermal annealing, its fluorescence spectrum is identical to that of pristine compound in solution. Similar features have been previously observed for related oligomers.[88]

ature is slightly different depending on the deposition process (absence of the low-energy emission band when spin-coated and presence of this band when vacuum-evaporated, Figure 4, bottom), which may be due to some close π–π interchromophore contacts of the pentaphenylene core. Hence, we believe that the large low-energy emission band arises from two different phenomena: π–π interchromophore interactions of the pentaphenylene unit and keto-defects due to the oxidation of the dialkyl bridgeheads.

The thermal properties of DSX-IF and DSX-LPP were finally evaluated by means of thermogravimetric analysis (Table 2). Decomposition temperature (T_d, corresponding to 5% loss) shows that both compounds exhibit very good thermal stabilities with high T_d (397 °C for DSX-IF and 380 °C for DSX-LPP), which is highly important to improve the lifetime of OLEDs. The xanthene derivatives DSX-LPP and DSX-IF present therefore a higher T_d compared with those of their 'all carbon' analogues, DSF-LPP and DSF-IF (365 and 355 °C, respectively).[53,54] Thus, the incorporation of xanthene units within indenofluorene and pentaphenylene units leads to molecules with enhanced thermal stability.

OLEDs with DSX-LPP and DSX-IF as emitting layers: To investigate the potential applications of DSX-LPP and DSX-IF as blue-emitting layers, several single-layer and multilayer OLEDs were fabricated and characterized. The energy-level diagrams and devices configuration of the different OLEDs are presented in the Supporting Information.

OLED performances: As there are only a few examples of nondoped OLEDs based on spiroxanthene oligomers in the literature,[51,52] we first decided to focus on single-layer devices to study the intrinsic properties of DSX-LPP and DSX-IF when used as the emitting layer (EML). Single-layer devices, ITO/PEDOT/DSX-IF or DSX-LPP/Ca (devices A) have been hence fabricated and their current density–voltage–luminance characteristics and luminous/energetic efficiencies are presented in the Supporting Information. The luminance of the single-layer device (device A) with DSX-IF (40 nm) as the EML reaches around 31 $Cd\,m^{-2}$ with luminous and energetic efficiencies of 8.10^{-3} $Cd\,A^{-1}$ and 2.10^{-3} $Lm\,W^{-1}$, respectively. These poor performances have been assigned to the wide gap of DSX-IF leading to a high injection barrier for both electrons and holes. The turn-on voltage of the device, defined as the voltage for a luminance of 1 $Cd\,m^{-2}$ is hence high, at around 12.7 V, translating the difficulty in injecting charges in DSX-IF.

The luminance of the single-layer device with DSX-LPP (50 nm) as EML reaches 220 $Cd\,m^{-2}$ (Table 3) signing hence a better injection of holes due to the higher HOMO level of DSX-LPP (−5.45 eV for DSX-LPP vs. −5.79 eV for DSX-IF). As the LUMO level of DSX-LPP is also lower than that of DSX-IF (−2.36 eV vs. −2.23 eV) the injection of electrons from the Ca cathode is also slightly improved. The turn-on voltage, 5.8 V, is therefore strongly decreased compared with that of DSX-IF device A and the efficiencies are impressively magnified by one order of magnitude (Table 3).

To improve the performances of the single-layer devices A, various double and triple-layer OLEDs were fabricated and characterized (devices B–D).

As DSX-IF possesses a relatively low HOMO level (−5.79 eV), it seemed appropriate to insert an intermediate layer of a hole transporter, namely NPB, to adjust its HOMO level with the HOMO level of the anode (−5.1 eV).

The turn-on voltage of the ITO/PEDOT/NPB (30 nm)/DSX-IF (40 nm)/Ca (device B) appears at approximately 10 V with a luminance impressively magnified by nearly two orders of magnitude, reaching approximately 2800 $Cd\,m^{-2}$ with luminous and energetic efficiencies of 0.6 $Cd\,A^{-1}$ and 0.16 $Lm\,W^{-1}$, respectively (Figure 7, top).[56] Device B presents performances impressively magnified by two orders of magnitude compared with those of device A (Table 3). Similarly, device B with DSX-LPP as the EML also leads to a strong enhancement of the performances (Figure 7, bottom). Indeed, the maximum luminance is recorded at approximately 1400 $Cd\,m^{-2}$ with a luminous efficiency of approximately 0.3 $Cd\,A^{-1}$. The performances of the DSX-LPP-based device B are lower than those of the DSX-IF-based device B exposed above. This might be explained by the fact that NPB presents a HOMO level lying at −5.4 eV, almost identical to that of DSX-LPP (−5.45 eV), but different to the low-lying HOMO level of DSX-IF (−5.79 eV). Thus, due to its HOMO level intermediate between that of PEDOT/PSS (−5.1 eV) and that of DSX-IF (−5.79 eV), NPB is hence more efficient in the case of DSX-IF than in

Table 3. Selected data of different devices investigated.

	Device	Turn-on voltage [V][a]	Maximum luminance [$Cd\,m^{-2}$]	Luminous efficiency [$Cd\,A^{-1}$][b]	Energetic efficiency [$Lm\,W^{-1}$][b]	Chromatic coordinates (x, y)	EL λ [nm]	Thickness of the organic layers [nm]
DSX-LPP	A	5.8	220	$8\times10^{-2}/4.5\times10^{-2}$	$4\times10^{-2}/1.5\times10^{-2}$	0.35, 0.38	403, 425, 452, 525, 558, 590	50
	B	8	1360	0.35/0.32	0.1/7 10^{-2}	0.30, 0.31	406, 425 (sh), 452, 525, 560	35/50
	C	5.9	398	$3.6\times10^{-2}/3.5\times10^{-2}$	$1.4\times10^{-2}/10^{-2}$	0.30, 0.28	404, 425, 452, 560	40/10
	D	10	1600	0.33/0.22	$9\times10^{-2}/4\times10^{-2}$	0.22, 0.22	404, 425, 452, 535, 560, 584 (sh)	35/40/10
DSX-IF	A	12.7	31	$8\times10^{-3}/5\times10^{-3}$	$2\times10^{-3}/10^{-3}$	0.18 , 0.08	413, 590, 650	40
	B	9.9	2770	0.6/0.4	0.16/0.08	0.19 , 0.08	414, 438, 590, 650	30/40
	C	7.3	190	$3.6\times10^{-2}/3.5\times10^{-2}$	$1.5\times10^{-2}/10^{-2}$	–	–	40/10
	D	8	3740	1/0.75	0.3/0.19	0.19, 0.14	413, 438, 590, 650	35/40/10

[a] For 1 $Cd\,m^{-2}$. [b] Left value: maximum value obtained, right value: efficiency at the maximum of luminance.

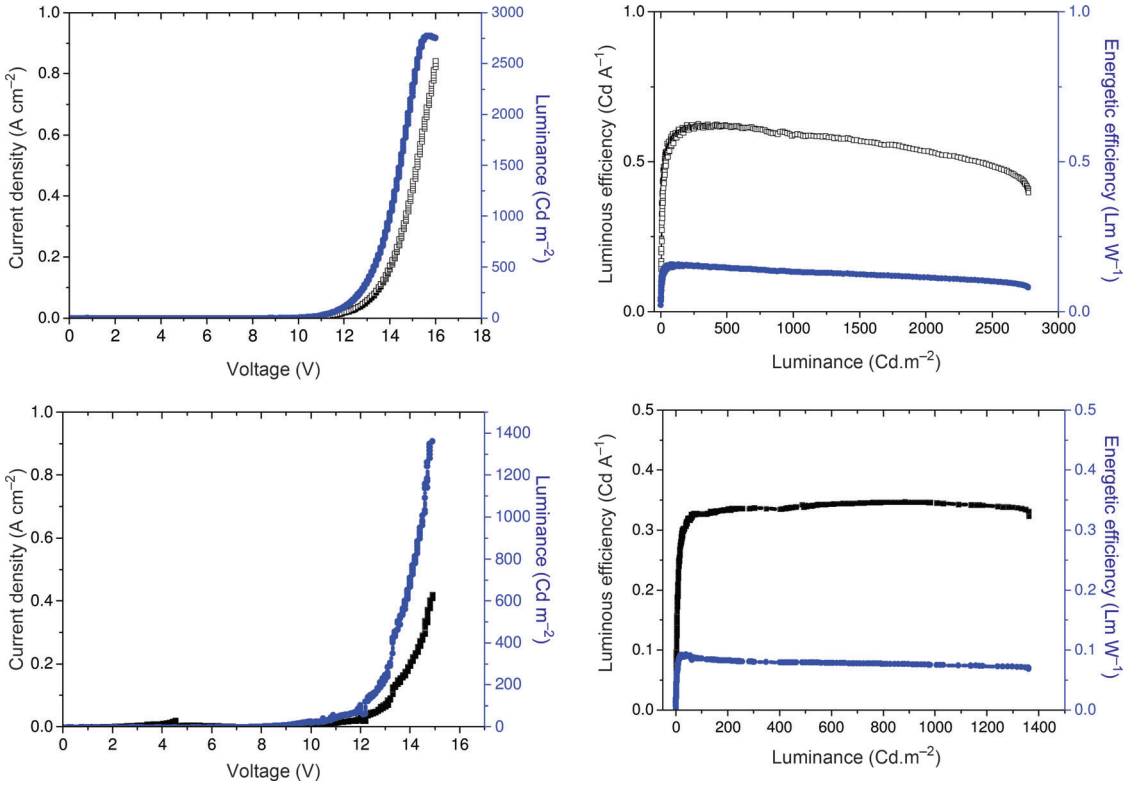

Figure 7. Current density–voltage–luminance characteristics (left) and luminous/energetic efficiencies (right) of devices B. Top) ITO/PEDOT/NPB (30 nm)/DSX-IF (40 nm)/Ca. Bottom) ITO/PEDOT/NPB (35 nm)/DSX-LPP (50 nm)/Ca.

the case of DSX-LPP. However, the performances of DSX-LPP-based device B are nevertheless better than those of device A because NPB avoids the quenching of the holes near the anode.

Finally, to prevent holes from crossing the device and reaching the cathode without recombination, a hole blocking layer (HBL) of bathocuproine (BCP, 2,9-dimethyl-4,7-diphenyl-1,10-phenanthroline) with a HOMO level of −6.4 eV[18,90,91] has been added (devices D).

The ITO/PEDOT/NPB/DSX-IF/BCP/Ca device D shows enhanced properties with a high luminance of approximately 3800 Cd m^{-2} at 12.5 V and efficiencies of 1 Cd A^{-1} and 0.3 Lm W^{-1} (Figure 8, top). The performances are hence almost doubled thanks to the insertion of BCP. As the device structure remains very simple and not-optimized, the NPB/DSX-IF/BCP system appears to be efficient compared to other simple blue OLEDs recently reported in the literature.[6,26,52]

Alas, the addition of BCP as a HBL in a DSX-LPP-based device (ITO/PEDOT/NPB/DSX-LPP/BCP/Ca: device D) does not lead to any impressive enhancement of the performances, which remain almost unchanged with a maximum luminance at 1600 Cd m^{-2} and a luminous efficiency of 0.33 Cd A^{-1} (Figure 8, bottom).

To find out about the influence of HBL, BCP was inserted between the emissive layer and the cathode in NPB-free devices (device C). The addition of BCP in the case of DSX-IF appears to be efficient. Indeed, device C presents an impressive decrease of the turn-on voltage from 12.7 V in the single-layer device A to 7 V in device C (see the Supporting Information). The luminance and resulting efficiencies are also enhanced by approximately one order of magnitude (see the Supporting Information) leading us to conclude that the BCP layer effectively avoids holes leakage and allows a better charge recombination in the DSX-IF layer.

For DSX-LPP, device C presents a turn-on voltage almost unchanged relative to the single-layer device A (5.9 V) and the luminance is doubled (~400 Cd m^{-2}). However, the efficiencies of device C do not vary much (see the Supporting Information).

In conclusion, the insertion of a HTL, namely NPB, leads to an impressive increase of the performances of DSX-LPP and DSX-IF-based devices. Thus, NPB appears to compensate unbalanced charge transport, both by enhancing holes transport and by preventing electrons from reaching the emissive layer/anode interface. Oppositely, the insertion of a HBL, namely BCP, has a less impressive effect on the performances of DSX-IF-based OLEDs and does not improve so much that of DSX-LPP-based OLEDs. In the case of DSX-LPP, this effect can be caused by a stronger unbalanced charge transport within the device than for DSX-IF. As BCP appears almost unnecessary for DSX-LPP-based devices, the holes do not need to be blocked at the DSX-LPP/Ca interface. This means that all the holes in the DSX-LPP layer recombine with electrons within the emissive layer. In the case of DSX-IF, there is a need for holes block-

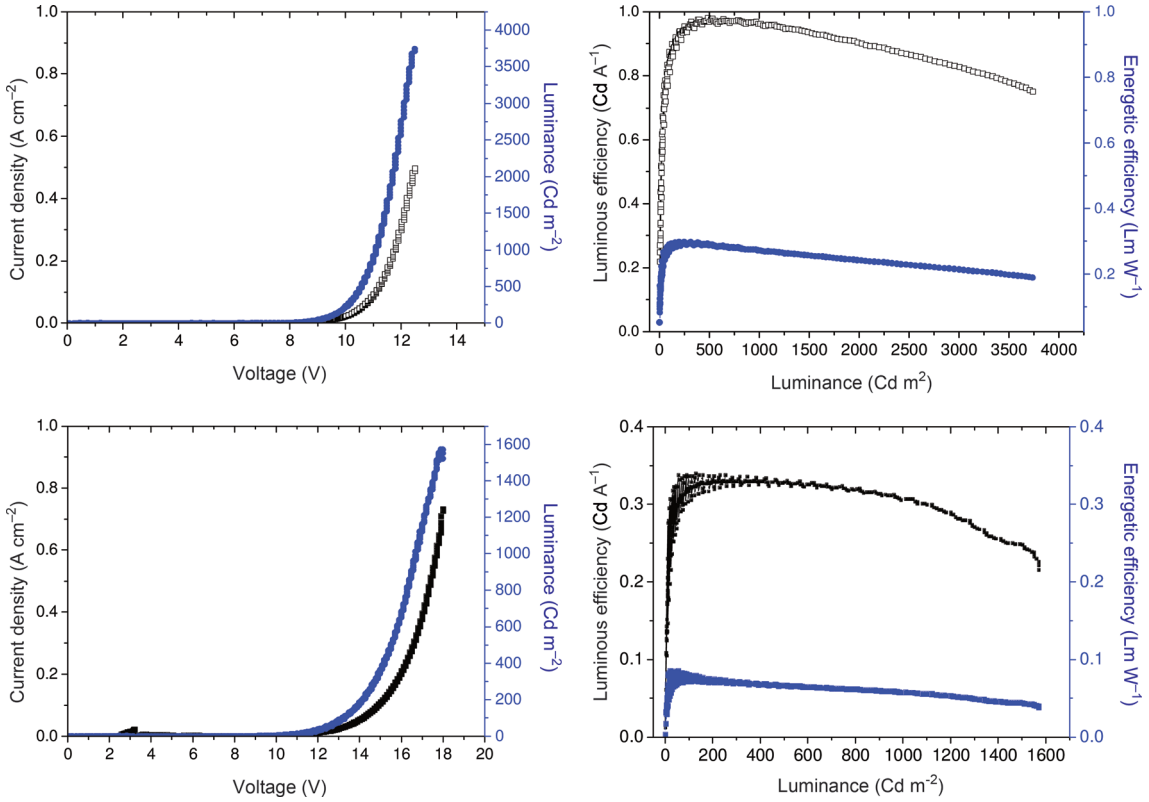

Figure 8. Current density–voltage–luminance characteristics (left) and luminous/energetic efficiencies (right) of devices D. Top) ITO/PEDOT/NPB (35 nm)/DSX-IF (40 nm)/BCP (10 nm)/Ca. Bottom) ITO/PEDOT/NPB (40 nm)/DSX-LPP (45 nm)/BCP (10 nm)/Ca.

ing, which means that either hole mobility is higher or electron mobility is lower.

Optical characterization: A detailed optical study of the different electroluminescence (EL) spectra is presented in this last part, with an emphasis 1) on the origin of the low-energy emission band observed in the case of DSX-LPP and 2) on the unexpected optical contribution of the well-known hole-transporting-layer NPB.

The normalized EL spectra of DSX-LPP- and DSX-IF-based devices are presented in Figure 9. All EL spectra of DSX-LPP-based devices are made of two main contributions: a blue one with two main peaks at around 403 and 425 nm due to the fluorescence of the pentaphenylene core and a green one with different maxima. The origin of these green low-energy emission bands observed in all the EL spectra of DSX-LPP-based devices will be discussed first.

Device A (Figure 9, top, ——) presents two main contributions: a sharp well-resolved contribution, in the blue region, with two maxima recorded at 403 and 425 nm in perfect accordance with the fluorescence spectrum of DSX-LPP (Figure 5, bottom) and a very broad contribution in the green region with three maxima recorded at 525, 558, and 590 nm. These two contributions in the EL spectrum of the single-layer device A leads to a pseudo-white color with chromatic coordinates of 0.35; 0.38 (see the CIE diagram in the Supporting Information). It is important to stress that a similar low-energy emission broad band was also observed in solid-state fluorescence studies after annealing in air (Figure 5, bottom). However, the relationship between the low-energy band observed in fluorescence and that observed in electroluminescence is clearly not evident as they may arise from different causes. First, because their maxima are different, and second because fluorescence and EL spectra have been obtained under very different conditions, that is, under an ambient atmosphere for the fluorescence spectra or under an inert atmosphere for the EL spectrum. At this early stage and in the light of literature, we can tentatively assign the green emission band observed in the EL spectrum of device A to intermolecular π–π stacking of the pentaphenylene units. Indeed, Müllen and co-workers have recently studied a very similar pentaphenylene derivative and have also reported the presence of a low-energy emission band in the EL spectrum, assigned to intermolecular π–π stacking.[71] However, the low-energy emission band observed in DSX-LPP-based devices seems to have multiple origins. Indeed, it is known in OLED technology that interactions between the electrodes (cathode and anode) and the EML may occur, and then the EL spectrum of the devices B and C, in which the cathode/anode is not directly in contact with the EML should be highly informative. The EL spectrum of device B (Figure 9, top, ——) with the anode covered with NPB presents the same broad band (λ_{max} = 523 and 558 nm) in the green region as that observed with device A, being, howev-

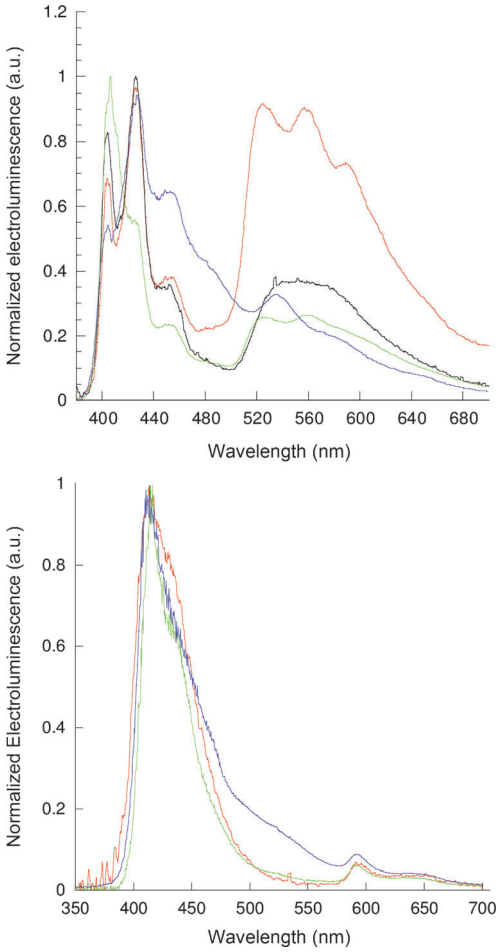

Figure 9. EL spectra of DSX-LPP-based devices (top ——: device A = ITO-PEDOT/DSX-LPP/Ca, ——: device B = ITO-PEDOT/NPB/DSX-LPP/Ca, ——: device C = ITO-PEDOT/DSX-LPP/BCP/Ca, ——: device D = ITO-PEDOT/NPB/DSX-LPP/BCP/Ca) and DSX-IF-based devices (bottom ——: device A = ITO-PEDOT/DSX-IF/Ca, ——: device B = ITO-PEDOT/NPB/DSX-IF/Ca, ——: device D = ITO-PEDOT/NPB/DSX-IF/BCP/Ca).

er, strongly decreased in intensity. Similarly, the EL spectrum of device C (Figure 9, top, ——) with the cathode covered with BCP, also presents a broad band in the green region but completely nonresolved, centered around 560 nm, and strongly reduced in intensity compared with that of device A. This is the proof that the low-energy emission band in the case of DSX-LPP-based devices arises from different causes. The first is clearly the Ca/EML interactions occurring in devices A and B, which are suppressed in device C. Indeed, such interactions are often seen despite the fact that the exact nature of the phenomenon has not been fully unraveled.[70] Similarly, the second cause is surely the interactions occurring between PEDOT/PSS and the EML. Indeed, such phenomena have been also previously suggested for similar extended π-conjugated backbones.[70] The EL spectrum of device D (Figure 9, top, ——), in which the electrodes are both covered by NPB and BCP clearly confirms that interactions occur between electrodes and the EML in devices A–C. Indeed, the EL spectrum of device D still possesses a green contribution but lower than that of devices A–C, assigned hence to intermolecular π–π stacking of DSX-LPP. Thus, the low-energy emission bands observed in all the DSX-LPP-based devices result from multiple origins, which renders the precise interpretation very complicated and notably their respective ratio. However, devices A–C present a color close to white, therefore making them highly interesting in lighting applications (see the CIE diagram in the Supporting Information).

The second important feature is related to the blue contributions in the EL spectra of the DSX-LPP- and DSX-IF-based devices.

In the case of DSX-LPP, devices A and C present EL spectra with two sharp bands at 403 and 425 nm (Figure 9, top), in accordance with its fluorescence spectra (Figure 5, bottom). In device B (with the NPB layer), these two bands are still observed but in a drastically different intensity ratio; the band at 403 nm being much more intense than that at 425 nm (Figure 9, top, ——). This difference seems to indicate a non-negligible contribution of the NPB layer in the EL spectra of DSX-LPP-based devices and leads us to go deeper in the knowledge of such systems. Indeed, despite being commonly used in OLED technology, reports describing the contribution of NPB in the EL spectra are very rare.[92] We hence first fabricated a single-layer device using NPB as the EML. The device ITO/NPB/Ca exhibits an extremely low luminance ($<10\ Cd\,m^{-2}$) and its EL spectrum presents a maximum at 415 nm (Figure 10, top). This value does not perfectly fit with that of the ITO/NPB/DSX-LPP/Ca device B (Figure 9, top, ——). To find out about the possible energy transfer between NPB and DSX-LPP, the fluorescence spectrum of a DSX-LPP/NPB blend (1:1 in weight) has been recorded and has shown the presence of a maximum at 405 nm (Figure 10, bottom, ——), in perfect accordance with the maximum observed 1) in the EL spectrum of the DSX-LPP-based device B (Figure 9, top, ——) and 2) in the fluorescence spectrum of the DSX-LPP thin-film (Figure 10, bottom, ——). Hence, the electron/hole recombination within the device appears to take place predominantly in the DSX-LPP layer but also slightly in the NPB layer. This recombination in two layers is probably due to the close HOMO/LUMO levels of both compounds (−5.45 eV/−2.36 eV for DSX-LPP and −5.4 eV/−2.3 eV for NPB). It is, however, obvious in the light of the interesting performances of the single-layer DSX-LPP-based device A (see above) and the very poor performances of the single layer NPB-based device, that the recombination predominantly takes place in the DSX-LPP layer. However, we believe that an energy transfer occurs between NPB and DSX-LPP leading hence to EL spectra containing a little contribution of the NPB layer.

In the case of DSX-IF, the contribution of the NPB layer appears to be more difficult to rationalize. Indeed, the normalized EL spectrum of the ITO/NPB/DSX-IF/Ca device B reveals two main peaks in the blue region, at 413 and 438 nm (Table 3), almost superimposable to the EL spec-

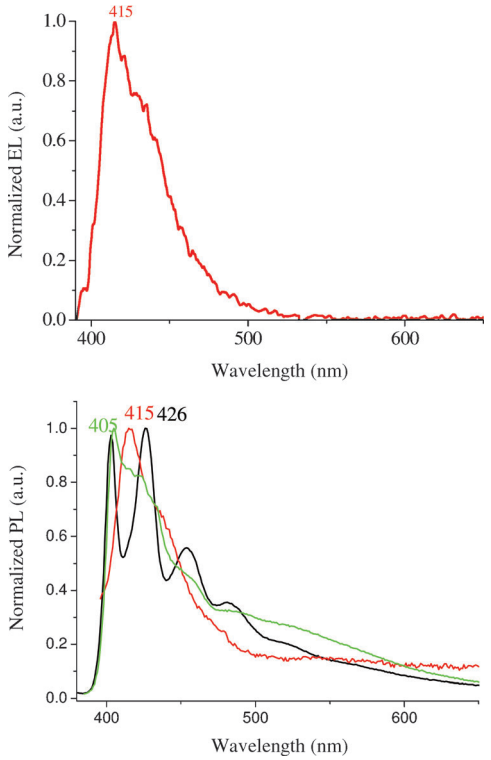

Figure 10. Top) EL spectra of the ITO/NPB/Ca device. Bottom) Fluorescence spectra ($\lambda_{exc}=370$ nm) of the spin-coated thin film of DSX-LPP (——), NPB (——), and a blend (1:1 in weight) of DSX-LPP/NPB (——).

trum of the ITO/DSX-IF/Ca device A (Figure 9, bottom, ——) but also almost superimposable to the EL spectrum of the ITO/NPB/Ca device (Figure 10, top). Thus, single-layer devices with DSX-IF or NPB as EML present surprisingly almost identical EL spectra.[3] It is, however, obvious that the good efficiencies obtained from DSX-IF-based devices cannot be attributed to the luminescence of NPB, even if an energy transfer may occur between NPB and DSX-IF, as depicted above in the case of DSX-LPP. The chromatic coordinates in the CIE 1964 chromaticity diagram calculated from the EL spectra of DSX-IF-based devices correspond to a blue color and are suitable for display applications (see the CIE diagram in the Supporting Information and Table 3).

Conclusion

In summary, we have designed and synthesized, through different and efficient synthetic approaches, very rigid spiro-configured blue fluorophores, DSX-LPP and DSX-IF, containing an intracyclic oxygen atom. Since the central π-conjugation is extended going from DSX-IF to DSX-LPP, we observed a gap contraction from 3.64 eV for DSX-IF to 3.25 eV for DSX-LPP. Compared with their 'all carbon' analogues, DSF-LPP and DSF-IF, xanthene derivatives DSX-LPP and DSX-IF showed enhanced thermal stability while maintaining similar optical (high quantum yield, blue fluorescence, and very small Stokes shift) and electrochemical properties. The xanthene-based materials hence appear promising for organic electronics applications as they could replace the 'all carbon' materials. The SMOLED application studies have been carried out with DSX-LPP and DSX-IF and have evidenced the potential of these new materials as emissive layers. For example, the nonoptimized three-layer DSX-IF-based device reaches a brightness of approximately 3800 $Cd\,m^{-2}$ with a maximum luminous efficiency of 1 $Cd\,A^{-1}$, which is promising for a blue fluorescent SMOLED (chromatic coordinates: 0.19; 0.14) and that can be further improved by adjusting the nature and the thicknesses of the different layers. Similarly, the nonoptimized double-layer DSX-LPP-based device reaches an interesting brightness of approximately 1400 $Cd\,m^{-2}$ with a maximum luminous efficiency of 0.35 $Cd\,A^{-1}$. A detailed optical study of the different EL spectra has been also carried out and has notably allowed us to conclude that the low-energy emission band observed in the EL spectra of DSX-LPP has multiple origins (interactions with anode and cathode and intermolecular π–π stacking) that cannot be directly linked to the fluorescence spectra. This work, which appears to be one of the rare examples of nondoped blue SMOLEDs based on xanthene derivatives, may pave the way to the development of this promising but very weakly studied class of materials.

Experimental Section

Synthesis: Commercially available reagents and solvents were used without further purification other than those detailed below. THF was distilled from sodium/benzophenone. Dichloromethane was distilled from P_2O_5 drying agent Sicapent (Merck). 1,2-Dichlorobenzene was distilled from $CaCl_2$ drying agent. Light petroleum refers to the fraction with b.p. 40–60 °C. Reactions were stirred magnetically, unless otherwise indicated. Analytical TLC was carried out by using aluminum-backed plates coated with Merck Kieselgel 60 GF_{254} and visualized under UV light (at 254 and/or 360 nm). Chromatography was carried out by using silica 60A CC 40–63 μm (SDS). ^1H and ^{13}C NMR spectra were recorded by using Bruker 300 MHz instruments (^1H frequency, corresponding ^{13}C frequency is 75 MHz); chemical shifts were recorded in ppm and J values in Hz. The residual signals for the NMR solvents are: $CDCl_3$, $\delta=7.26$ for the proton and 77.00 ppm for the carbon. The following abbreviations have been used for the NMR spectroscopic assignments: s for singlet, d for doublet, t for triplet, q for quintet, and m for multiplet. HRMS were recorded either at the Centre Régional de Mesures Physiques de l'Ouest (Rennes) or with a Microflex LT (Bruker). Diketones **1** and **3** and 2,2"-DITP were prepared in a multistep synthesis as previously reported.[53,54] Full characterization of DSX-IF can be found in our preliminary note.[56] Names of chemicals have been generated with the naming service of ACD-I lab, which determines the chemical name according to systematic application of the nomenclature rules agreed upon by the International Union of Pure and Applied Chemistry and International Union of Biochemistry and Molecular Biology.

Dispiro(xanthene-9,6′-indeno[1,2−*b*]fluorene-12′,9"-xanthene) (DSX-IF): In a schlenk tube under an argon atmosphere, 2,2"-DITP (0.30 g,

[3] It should be noted that DSX-IF-based OLEDs also present a small contribution in the red region (590/650 nm) attributed to interactions with the calcium cathode. Indeed, switching to LiF/Al instead of Ca leads to the complete disappearance of this band (see the Supporting Information).

0.63 mmol) was dissolved in dry THF (7 mL) and the solution was degassed. The mixture was cooled to −78 °C and stirred at this temperature for 10 min. A solution of *n*BuLi (1.6 M in hexane, 1.6 mL, 2.56 mmol) was added dropwise over 3.5 min. The resulting cloudy yellow solution was stirred for a further 3.5 min and xanthone (0.27 g, 1.37 mmol), dissolved in dry and degassed THF (20 mL), was added dropwise over 4 min by a cannula. The reaction was allowed to stir overnight (from −70 °C to room temperature) and the resulting mixture was poured into a saturated solution of ammonium chloride (10 mL) and THF (20 mL) was added before extraction with dichloromethane. The combined extracts were dried ($MgSO_4$) and the solvent was removed in vacuo. The resulting crude mixture was taken up with dichloromethane/light petroleum (8:2) and filtered to afford the dixanthenol intermediate as a pure product. This dixanthenol was then suspended in acetic acid (30 mL) with concentrated hydrochloric acid (0.5 mL). The resulting mixture was allowed to stir for 90 min at 100 °C and water (30 mL) was added. After cooling to room temperature, the colorless precipitate was filtered to afford the title compound DSX-IF as a colorless solid (0.18 g, 50 %). Elemental analysis calcd (%) for $C_{44}H_{26}O_2$: C 90.08, H 4.47; found: C 89.48, H 4.55. The spectroscopic analyses and purity of DSX-IF were in perfect accordance with our previous work.[56]

9′,9′,18′,18′-Tetraoctyl-9′,18′-dihydrodispiro(xanthene-9,6′-benzo-[5,6*s*]indaceno[1,2-*b*]indeno[2,1*h*]fluorene-15′,9″-xanthene) (DSX-LPP): A mixture of 9,9,18,18-tetraoctyl-9,18-dihydrobenzo[5,6]-*s*-indaceno[1,2-*b*]indeno[2,1*h*]fluorene-6,15-dione (**1**)[54] (200 mg, 0.2 mmol), phenol (414 mg, 4.0 mmol), and methane sulfonic acid (114 μL, 170 mg, 1.8 mmol) in 1,2-dichlorobenzene (20 mL) was heated at 160 °C under an argon atmosphere for 24 h. The reaction was quenched with water (30 mL) and the mixture extracted with dichloromethane (3×10 mL). The extracts were dried over $MgSO_4$. The solvent was removed in vacuo and the residue was purified by column chromatography on silica gel eluting with dichloromethane/light petroleum (1:4) to give the title compound (143 mg, 54 %) as a colorless solid. M.p. = 287 °C (MeCN); R_f = 0.4 (dichloromethane/light petroleum (1:9), ^{1}H NMR (300 MHz; $CDCl_3$) δ = 7.54 (d, J = 3 Hz, 4H; ArH), 7.49–7.47 (m, 2H; ArH), 7.42 (s, 2H; ArH), 7.38–7.34 (dd, J = 8.4 Hz, J = 1.5 Hz, 4H; ArH), 7.31–7.20 (m, 10H; ArH), 6.87–6.82 (td, J = 7.4 Hz, J = 1.5 Hz, 4H; ArH), 6.57–6.54 ppm (dd, J = 7.4 Hz, J = 1.5 Hz, 4H; ArH), 1.98 (t, J = 7.2 Hz, 8H; CH_2), 1.25–0.98 (m, 40H; CH_2), 0.79 (t, J = 7.2 Hz, 12H; Me), 0.70–0.54 ppm (m, 8H; CH_2); ^{13}C NMR (75 MHz; CD_2Cl_2) δ = 156.1 (C), 154.0 (C), 151.6 (C), 151.2 (C), 150.9 (C), 141.7 (C), 140.8 (C), 139.6 (C), 139.6 (C), 128.5 (C), 128.1 (CH), 126.9 (CH), 126.6 (CH), 125.7 (CH), 123.4 (CH), 122.8 (CH), 119.7 (CH), 117.0 (CH), 116.8 (CH), 116.7 (CH), 114.3 (CH), 54.9 (C), 53.7 (C), 40.6 (CH_2), 31.7 (CH_2), 30.0 (CH_2), 29.2 (CH_2), 29.2 (CH_2), 23.8 (CH_2), 22.6 (CH_2), 14.0 ppm (Me); IR (KBr): $\tilde{\nu}$ = 2926, 2853, 1600, 1571, 1477, 1441, 1415, 1285, 1244 cm^{-1} (Ph–O); HRMS (ESI): m/z: calcd for $C_{90}H_{98}O_2$+Na: 1233.74645 $[M+Na]^+$; found: 1233.7429; elemental analysis calcd (%) for $C_{90}H_{98}O_2$: C 89.21, H 8.15; found: C 89.12, H 8.14.

4,4′,4″,4‴-(9,9,18,18-Tetraoctyl-6,9,15,18-tetrahydrobenzo[5,6]-*s*-indaceno-[1,2-*b*]indeno[2,1*h*]fluorene-6,6,15,15-tetrayl)tetraphenol (2): A mixture of 9,9,18,18-tetraoctyl-9,18-dihydrobenzo[5,6]-*s*-indaceno[1,2-*b*]indeno-[2,1*h*]fluorene-6,15-dione (**1**)[54] (70 mg, 0.08 mmol), phenol (75 mg, 0.8 mmol), and methane sulfonic acid (52 μL, 76 mg, 0.8 mmol) was heated at 160 °C under an argon atmosphere for 12 h. The reaction was quenched with water (30 mL) and the mixture extracted with dichloromethane (5×10 mL). The extracts were dried over $MgSO_4$. The solvent was removed in vacuo and the residue was purified by column chromatography on silica gel eluting with dichloromethane/AcOEt (95:5) to give the title compound (25 mg, 26 %) as a colorless solid; ^{1}H NMR (300 MHz; $CDCl_3$): δ = 7.99 (d, J = 7.5 Hz, 4H; ArH), 7.51–7.46 (m, 6H; ArH), 7.35 (d, J = 8.4 Hz, 2H; ArH), 7.28–7.11 (m, 12H; ArH), 6.95 (s, 2H; ArH), 6.90 (d, J = 7.5 Hz, 4H; ArH), 1.91 (t, J = 7.2 Hz, 8H; CH_2), 1.55 (s, 4H; OH), 1.35–1.02 (m, 40H; CH_2), 0.79 (t, J = 7.2 Hz, 12H; Me), 0.67–0.47 ppm (m, 8H; CH_2); ^{13}C NMR (75 MHz; $CDCl_3$): δ = 151.0 (C), 150.8 (C), 149.6 (C), 149.1 (C), 147.8 (C), 141.9 (C), 141.9 (C), 141.0 (C), 140.9 (C), 140.8 (C), 127.9 (CH), 127.7 (CH), 126.6 (CH), 126.4 (CH), 124.4 (CH), 122.6 (CH), 120.1 (CH), 119.6 (CH), 115.2 (CH), 115.0 (CH), 114.4 (CH), 65.6 (C), 54.7 (C), 40.6 (CH_2), 31.7 (CH_2), 30.0 (CH_2), 29.7 (CH_2), 29.2 (CH_2), 23.7 (CH_2), 22.6 (CH_2), 14.0 ppm (Me); HRMS (ESI): m/z: calcd for $C_{90}H_{102}O_4$: 1246.77781 $[M]^+$; found: 1246.7774.

X-ray analysis: Crystal data of DSX-LPP are presented below. The crystal was picked up with a cryoloop and then frozen at 100 K under a stream of dry N_2 on a APEX II Brucker AXS diffractometer for X-ray data collection ($Mo_{K\alpha}$ radiation, λ = 0.71073 Å). The structure was solved by direct methods (SIR97),[93] and then refined by full-matrix least-square methods based on F^2 (SHELXL-97)[94] as implemented in the WinGX software package.[95] An empirical absorption correction was applied. Hydrogen atoms were introduced at calculated positions (riding model) included in structure factor calculation but not refined. CCDC-816681 contains the supplementary crystallographic data for this paper. These data can be obtained free of charge from The Cambridge Crystallographic Data Centre via www.ccdc.cam.ac.uk/data_request/cif.

Data for DSX-LPP: $C_{92}H_{100}Cl_6O_2$; M = 1450.42; pale-yellow prism; crystal size = 0.4×0.4×0.3 mm; triclinic; $P\bar{1}$; a = 12.1508(6), b = 12.7242(6), c = 13.5848(7) Å; α = 95.064(2), β = 109.720(2), γ = 98.741(2)°; V = 1932.09(17) Å^3; Z = 1; ρ_{calcd} = 1.247 Mg m^{-3}; $Mo_{K\alpha}$ radiation λ = 0.71073 Å; μ = 0.272 mm^{-1}; T = 100 K; 24060 data (8746 unique, R_{int} = 0.0297, 1.61 < θ < 27.50°); $wR = \{\Sigma[w(F_o^2-F_c^2)^2]/\Sigma[w(F_o^2)^2]\}^{1/2}$ = 0.1403; conventional R = 0.0446 for F values of reflections with $F_o^2 > 2\sigma(F_o^2)$ (7565 observed reflections); S = 1.066 for 451 parameters. Residual electron density extremes were 0.563 and −0.417 e Å^{-3}.

Spectroscopic studies: Pyridine was purchased from Acros. Toluene (semiconductor grade) was purchased from Alfa Aesar. DSX-IF (10 mg mL^{-1} in pyridine, 90 μL) and DSX-LPP (20 mg mL^{-1} in toluene, 90 μL) were deposited on a quartz substrate by using a 'home made' spin coater and UV/Vis and photoluminescence spectra were immediately recorded. UV/Vis spectra were recorded by using a UV/Vis spectrophotometer SHIMADZU UV-1605. The optical gap was calculated from the absorption edge of the UV/Vis absorption spectrum by using the formula ΔE^{opt} (eV) = hc/λ, in which λ is the absorption edge (in meters), h = 6.6262×10^{-34} J s (1 eV = 1.602×10^{-19} J), and c = 2.99×10^8 m s^{-1} (ΔE^{opt} (eV) = 1237.5/λ (nm). Photoluminescence spectra were recorded with a PTI spectrofluorimeter (PTI-814 PDS, MD 5020, LPS 220B) by using a xenon lamp either in solution (cyclohexane) or in thin-film. Quantum yields in solution (λ_{sol}) were calculated relative to quinine sulfate (λ_{sol} = 0.546 in H_2SO_4 1 N) by using standard procedures.[2] λ_{sol} was determined according to Equation (1):

$$\phi_{sol} = \phi_{ref} \times 100 \times \frac{(T_s \times A_r)}{(T_r \times A_s)} \left(\frac{n_s}{n_r}\right)^2 \quad (1)$$

in which subscripts s and r refer to the sample and reference, respectively. The integrated area of the emission peak in arbitrary units is given as T, n is the refracting index of the solvent (n_s = 1.42662 for cyclohexane), and A is the absorbance ($\leq$0.1). IR spectra were recorded on a BIORAD IRFTS175C.

Thermal analysis: Thermogravimetric analyses (TGA) were carried out with a Rigaku Thermoflex instrument under a nitrogen atmosphere between room temperature up to 1000 °C with a heating rate of 5 °C min^{-1}. Melting points were determined by using an electrothermal melting-point apparatus.

Electrochemical studies: All electrochemical experiments were performed under an argon atmosphere by using a Pt disk electrode (diameter 1 mm), the counter electrode was a vitreous carbon rod and the reference electrode was a silver wire in a 0.1 M $AgNO_3$ solution in CH_3CN. Ferrocene was added to the electrolyte solution at the end of a series of experiments. The ferrocene/ferrocenium (Fc/Fc^+) couple served as an internal standard. The three-electrode cell was connected to a PAR Model 273 potentiostat/galvanostat (PAR, EGandG, USA) monitored with the ECHEM software. Dichloromethane with less than 100 ppm of water (ref. SDS 02910E21) were used without purification. Activated Al_2O_3 was added in the electrolytic solution to remove excess moisture. For a further comparison of the electrochemical and optical properties, all potentials are referred to the SCE electrode that was calibrated at −0.405 V versus the Fc/Fc^+ system. By following the work of Jenekhe,[77]

we estimated the electron affinity (EA) or LUMO and the ionization potential (IP) or HOMO from the redox data. The LUMO level was calculated from: LUMO (eV) = $-[E^{red}_{onset}$ (vs SCE) $+4.4]$ and the HOMO level from: HOMO (eV) = $-[E^{ox}_{onset}$ (vs SCE) $+4.4]$, based on an SCE energy-level of 4.4 eV relative to the vacuum. The electrochemical gap was calculated from $\Delta E^{el} = |$HOMO–LUMO$|$ (in eV).

EL fabrication and testing: OLEDs were fabricated by using the following procedure. Indium–tin oxide (ITO) substrates on glass from Merck underwent a solvent ultrasonic cleansing by using acetone and isopropanol followed by a 15 min UV–ozone treatment. A layer of poly(3,4-ethylene dioxythiophene) doped with poly(styrene sulfonate) (PEDOT/PSS from HC Starck) was then deposited onto ITO by spin-coating at 5000 rpm, from a 3 wt.% water dispersion to form a 40 nm-thick layer. PEDOT/PSS was subsequently annealed at 80°C under vacuum for 30 min. This layer improves hole injection from the ITO to the HOMO level of the organic material and increases the performances and the lifetime of the device. Then, NPB, DSX-IF, DSX-LPP, and finally BCP layers were thermally evaporated under vacuum (ca. 10^{-6} mbar) at deposition rates of 5 Å min^{-1}. The layer thickness was monitored in-situ during the evaporation by a piezoelectric quartz. Calcium cathodes were finally evaporated through a shadow mask. The OLEDs were then stored and characterized under an inert atmosphere in a nitrogen glove box ($[O_2]$ and $[H_2O] < 1$ ppm). Contacts on ITO and Ca were taken by using a prober (Karl Suss PM5). Current—voltage–luminance (I–V–L) curves were recorded by using a Keithley 4200 SCS. Light emission was collected by using a calibrated photodiode. Electroluminescence spectra were measured with a CCD spectrometer (Ocean Optics HR 2000).

Acknowledgements

N.C. thanks the MENRT for a studentship. We wish to highly thank Dr. N. Audebrand for TGA analyses (UMR CNRS, 6226-Rennes), the CDIFX (Centre de Diffractométrie X-Rennes) for data collections, the C.R.M.P.O (Centre Régional de Mesure Physique de l'Ouest) for HRMS, the Service de Microanalyse-CNRS (Gif sur Yvette) for CHN analyses, Sokha Khiev for some OLED fabrication, and D. Thirion for his efficient contribution.

[1] Special issue: π-Functional Materials, J. L. Bredas, S. R. Marder, E. Reichmanis, *Chem. Mater.* **2011**, *23*, Issue 3.
[2] Special issue: Organic Electronics and Optoelectronics, S. R. Forrest, M. E. Thompson, *Chem. Rev.* **2007**, *107*, Issue 4.
[3] A. C. Grimsdale, K. L. Chan, R. E. Martin, P. G. Jokisz, A. B. Holmes, *Chem. Rev.* **2009**, *109*, 897–1091.
[4] *Organic Light-Emitting Devices: Synthesis, Properties and Applications* (Eds.: K. Müllen, U. Scherf), Wiley-VCH, Weinheim, **2006**.
[5] B. Geffroy, P. Le Roy, C. Prat, *Polym. Int.* **2006**, *55*, 572–582.
[6] F. Liu, L.-H. Xie, C. Tang, J. Liang, Q.-Q. Chen, B. Peng, W. Wei, Y. Cao, W. Huang, *Org. Lett.* **2009**, *11*, 3850–3853.
[7] S.-K. Kim, B. Yang, Y. Ma, J.-H. Lee, J.-W. Park, *J. Mater. Chem.* **2008**, *18*, 3376–3384.
[8] S. Liu, F. He, H. Wang, H. Xu, C. Wang, F. Li, Y. Ma, *J. Mater. Chem.* **2008**, *18*, 4802–4807.
[9] T. Qin, G. Zhou, H. Scheiber, R. E. Bauer, M. Baumgarten, C. E. Anson, E. J. W. List, K. Müllen, *Angew. Chem.* **2008**, *120*, 8416–8420; *Angew. Chem. Int. Ed.* **2008**, *47*, 8292–8296.
[10] J. N. Moorthy, P. Venkatakrishnan, P. Natarajan, D.-F. Huang, T. J. Chow, *J. Am. Chem. Soc.* **2008**, *130*, 17320–17333.
[11] A. S. Ionkin, W. J. Marshall, B. M. Fish, L. M. Bryman, Y. Wang, *Chem. Commun.* **2008**, 2319–2321.
[12] Y.-I. Park, J.-H. Son, J.-S. Kang, S.-K. Kim, J.-H. Lee, J.-W. Park, *Chem. Commun.* **2008**, 2143–2145.
[13] M.-Y. Lai, C.-H. Chen, W.-S. Huang, J. T. Lin, T.-H. Ke, L.-Y. Chen, M.-H. Tsai, C.-C. Wu, *Angew. Chem.* **2008**, *120*, 591–595; *Angew. Chem. Int. Ed.* **2008**, *47*, 581–585.
[14] A. Goel, S. Chaurasia, M. Dixit, V. Kumar, S. Prakash, B. Jena, J. K. Verma, M. Jain, R. S. Anand, S. S. Manoharan, *Org. Lett.* **2009**, *11*, 1289–1292.
[15] Q.-X. Tong, S.-L. Lai, M.-Y. Chan, Y.-C. Zhou, H.-L. Kwong, C. S. Lee, S.-T. Lee, T.-W. Lee, T. Noh, O. Kwon, *J. Phys. Chem. C* **2009**, *113*, 6227–6230.
[16] C.-H. Wu, C.-H. Chien, F.-M. Hsu, P.-I. Shih, C.-F. Shu, *J. Mater. Chem.* **2009**, *19*, 1464–1470.
[17] Z. Jiang, H. Yao, Z. Liu, C. Yang, C. Zhong, J. Qin, G. Yu, Y. Liu, *Org. Lett.* **2009**, *11*, 4132–4135.
[18] C.-C. Chi, C.-L. Chiang, S.-W. Liu, H. Yueh, C.-T. Chen, C.-T. Chen, *J. Mater. Chem.* **2009**, *19*, 5561–5571.
[19] H.-Y. Chen, C.-T. Chen, C.-T. Chen, *Macromolecules* **2010**, *43*, 3613–3623.
[20] H. Li, A. S. Batsanov, K. C. Moss, H. L. Vaughan, F. B. Dias, K. T. Kamtekar, M. R. Bryce, A. P. Monkman, *Chem. Commun.* **2010**, *46*, 4812–4814.
[21] J. N. Moorthy, P. Venkatakrishnan, P. Natarajan, Z. Lin, T. J. Chow, *J. Org. Chem.* **2010**, *75*, 2599–2609.
[22] L.-O. Pålsson, C. Wang, A. S. Batsanov, S. M. King, A. Beeby, A. P. Monkman, M. R. Bryce, *Chem. Eur. J.* **2010**, *16*, 1470–1479.
[23] Y. Park, S. Kim, J.-H. Lee, D. H. Jung, C.-C. Wu, J. Park, *Org. Electron.* **2010**, *11*, 864–871.
[24] J.-L. Wang, Y. Zhou, Y. Li, J. Pei, *J. Org. Chem.* **2009**, *74*, 7449–7456.
[25] S. Ye, J. Chen, C.-a. Di, Y. Liu, K. Lu, W. Wu, C. Du, Y. Liu, Z. Shuai, G. Yu, *J. Mater. Chem.* **2010**, *20*, 3186–3194.
[26] J. Wang, W. Wan, H. Jiang, Y. Gao, X. Jiang, H. Lin, W. Zhao, J. Hao, *Org. Lett.* **2010**, *12*, 3874–3877.
[27] Z. Ma, P. Sonar, Z.-K. Chen, *Curr. Org. Chem.* **2010**, *14*, 2034–2069.
[28] T. Qin, W. Wiedemair, S. Nau, R. Trattnig, S. Fax, S. Winkler, A. Vollmer, N. Koch, M. Baumgarten, E. J. W. List, K. Müllen, *J. Am. Chem. Soc.* **2011**, *133*, 1301–1304.
[29] H. Huang, Q. Fu, S. Zhuang, Y. Liu, L. Wang, J. Chen, D. Ma, C. Yang, *J. Phys. Chem. C* **2011**, *115*, 4872–4878.
[30] R. Grisorio, G. Melcarne, G. P. Suranna, P. Mastrorilli, C. F. Nobile, P. Cosma, P. Fini, S. Colella, E. Fabiano, M. Piacenza, F. Della Sala, G. Ciccarella, M. Mazzeo, G. Gigli, *J. Mater. Chem.* **2010**, *20*, 1012–1018.
[31] T. P. I. Saragi, T. Spehr, A. Siebert, T. Fuhrmann-Lieker, J. Salbeck, *Chem. Rev.* **2007**, *107*, 1011–1065.
[32] L.-H. Xie, J. Liang, J. Song, C.-R. Yin, W. Huang, *Curr. Org. Chem.* **2010**, *14*, 2169–2195.
[33] J. Salbeck, F. Weissörtel, J. Bauer, *Macromol. Symp.* **1998**, *125*, 121–132.
[34] S. Tang, M. Liu, P. Lu, H. Xia, M. Li, Z. Xie, F. Z. Shen, C. Gu, H. Wang, B. Yang, Y. Ma, *Adv. Funct. Mater.* **2007**, *17*, 2869–2877.
[35] Y.-L. Liao, C.-Y. Lin, K.-T. Wong, T.-H. Hou, W.-Y. Hung, *Org. Lett.* **2007**, *9*, 4511–4514.
[36] K.-S. Kim, H. S. Lee, Y.-M. Jeon, J.-W. Kim, C.-W. Lee, M.-S. Gong, *Dyes Pigm.* **2009**, *81*, 174–179.
[37] S. Tang, M. Liu, P. Lu, G. Cheng, M. Zeng, Z. Xie, H. Xu, H. Wang, B. Yang, Y. Ma, D. Yan, *Org. Electron.* **2008**, *9*, 241–252.
[38] T. Lei, J. Luo, L. Wang, Y. Ma, J. Wang, Y. Cao, J. Pei, *New J. Chem.* **2010**, *34*, 699–707.
[39] S. Tang, M. Liu, C. Gu, Y. Zhao, P. Lu, D. Lu, L. Liu, F. Shen, B. Yang, Y. Ma, *J. Org. Chem.* **2008**, *73*, 4212–4218.
[40] K.-S. Kim, Y.-M. Jeon, J.-W. Kim, C.-W. Lee, M.-S. Gong, *Org. Electron.* **2008**, *9*, 797–804.
[41] J. Luo, Y. Zhou, Z.-Q. Niu, Q.-F. Zhou, Y. Ma, J. Pei, *J. Am. Chem. Soc.* **2007**, *129*, 11314–11315.
[42] T. Kowada, Y. Matsuyama, K. Ohe, *Synlett* **2008**, 1902–1906.
[43] T. Kowada, T. Kuwabara, K. Ohe, *J. Org. Chem.* **2010**, *75*, 906–913.
[44] M. Miyasaka, M. Pink, S. Rajca, A. Rajca, *Org. Lett.* **2010**, *12*, 3230–3233.
[45] K.-T. Wong, H.-F. Chen, F.-C. Fang, *Org. Lett.* **2006**, *8*, 3501–3504.
[46] K.-T. Wong, R.-T. Chen, F.-C. Fang, C.-c. Wu, Y.-T. Lin, *Org. Lett.* **2005**, *7*, 1979–1982.

[47] J. Londenberg, T. P. I. Saragi, I. Suske, J. Salbeck, *Adv. Mater.* **2007**, *19*, 4049–4053.
[48] Y.-H. Tseng, P.-I. Shih, C.-H. Chien, A. K. Dixit, C.-F. Shu, Y.-H. Liu, G.-H. Lee, *Macromolecules* **2005**, *38*, 10055–10060.
[49] D. Vak, S. J. Shin, J.-H. Yum, S.-S. Kim, D.-Y. Kim, *J. Lumin.* **2005**, *115*, 109–116.
[50] S. L. McFarlane, L. S. Coumont, D. G. Piercey, R. McDonald, J. G. C. Veinot, *Macromolecules* **2008**, *41*, 7780–7782.
[51] J.-F. Gu, G.-H. Xie, L. Zhang, S.-F. Chen, Z.-Q. Lin, Z.-S. Zhang, J.-F. Zhao, L.-H. Xie, C. Tang, Y. Zhao, S.-Y. Liu, W. Huang, *J. Phys. Chem. Lett.* **2010**, *1*, 2849–2853.
[52] Z. Chu, D. Wang, C. Zhang, X. Fan, Y. Tang, L. Chen, D. Zou, *Macromol. Rapid Commun.* **2009**, *30*, 1745–1750.
[53] C. Poriel, J.-J. Liang, J. Rault-Berthelot, F. Barrière, N. Cocherel, A. M. Z. Slawin, D. Horhant, M. Virboul, G. Alcaraz, N. Audebrand, L. Vignau, N. Huby, L. Hirsch, G. Wantz, *Chem. Eur. J.* **2007**, *13*, 10055–10069.
[54] N. Cocherel, C. Poriel, J. Rault-Berthelot, F. Barrière, N. Audebrand, A. M. Z. Slawin, L. Vignau, *Chem. Eur. J.* **2008**, *14*, 11328–11342.
[55] A. C. Grimsdale, K. Müllen, *Macromol. Rapid Commun.* **2007**, *28*, 1676–1702.
[56] N. Cocherel, C. Poriel, L. Vignau, J.-F. Bergamini, J. Rault-Berthelot, *Org. Lett.* **2010**, *12*, 452–455.
[57] J. Jacob, J. Zhang, A. C. Grimsdale, K. Müllen, M. Gaal, E. J. W. List, *Macromolecules* **2003**, *36*, 8240–8245.
[58] D. Marsitzky, J. C. Scott, J.-P. Chen, V. Y. Lee, R. D. Miller, S. Setayesh, K. Müllen, *Adv. Mater.* **2001**, *13*, 1096–1099.
[59] S.-Y. Ku, L.-C. Chi, W.-Y. Hung, S.-W. Yang, T.-C. Tsai, K.-T. Wong, Y.-H. Chen, C.-I. Wu, *J. Mater. Chem.* **2009**, *19*, 773–780.
[60] L.-C. Chi, W.-Y. Hung, H.-C. Chiu, K.-T. Wong, *Chem. Commun.* **2009**, 3892–3894.
[61] S. Merlet, M. Birau, Z. Y. Wang, *Org. Lett.* **2002**, *4*, 2157–2159.
[62] T.-C. Lin, C.-S. Hsu, C.-L. Hu, Y.-F. Chen, W.-J. Huang, *Tetrahedron Lett.* **2009**, *50*, 182–185.
[63] W. Zhang, J. Smith, R. Hamilton, M. Heeney, J. Kirkpatrick, K. Song, S. E. Watkins, T. Anthopoulos, I. McCulloch, *J. Am. Chem. Soc.* **2009**, *131*, 10814–10815.
[64] H. Usta, C. Risko, Z. Wang, H. Huang, M. K. Deliomeroglu, A. Zhukhovitskiy, A. Facchetti, T. J. Marks, *J. Am. Chem. Soc.* **2009**, *131*, 5586–5608.
[65] H. Usta, A. Facchetti, T. J. Marks, *J. Am. Chem. Soc.* **2008**, *130*, 8580–8581.
[66] L. Romaner, G. Heimel, H. Wiesenhofer, P. Scanducci de Freitas, U. Scherf, J. L. Bredas, E. Zojer, E. J. W. List, *Chem. Mater.* **2004**, *16*, 4667–4674.
[67] C. Xia, R. C. Advincula, *Macromolecules* **2001**, *34*, 6922–6928.
[68] Q. Zheng, S. K. Gupta, G. S. He, L.-S. Tan, P. N. Prasad, *Adv. Funct. Mater.* **2008**, *18*, 2770–2779.
[69] J. Jacob, S. Sax, M. Gaal, E. J. W. List, A. C. Grimsdale, K. Müllen, *Macromolecules* **2005**, *38*, 9933–9938.
[70] A. K. Mishra, M. Graf, F. Grasse, J. Jacob, E. J. W. List, K. Müllen, *Chem. Mater.* **2006**, *18*, 2879–2885.
[71] C. E. Finlayson, J.-S. Kim, M. Liddell, R. H. Friend, S.-H. Jung, A. C. Grimsdale, K. Müllen, *J. Chem. Phys.* **2008**, *128*, 044703.
[72] Y. Wu, J. Zhang, Z. Bo, *Org. Lett.* **2007**, *9*, 4435–4438.
[73] J. Jacob, S. Sax, T. Piok, E. J. W. List, A. C. Grimsdale, K. Müllen, *J. Am. Chem. Soc.* **2004**, *126*, 6987–6995.
[74] N. Cocherel, C. Poriel, O. Jeannin, A. Yassin, J. Rault-Berthelot, *Dyes Pigm.* **2009**, *83*, 339–347.
[75] L.-H. Xie, F. Liu, C. Tang, X.-Y. Hou, Y.-R. Hua, Q.-L. Fan, W. Huang, *Org. Lett.* **2006**, *8*, 2787–2790.
[76] L.-H. Xie, X.-Y. Hou, C. Tang, Y.-R. Hua, R.-J. Wang, R.-F. Chen, Q.-L. Fan, L.-H. Wang, W. Wei, B. Peng, W. Huang, *Org. Lett.* **2006**, *8*, 1363–1366.
[77] A. P. Kulkarni, C. J. Tonzola, A. Babel, S. A. Jenekhe, *Chem. Mater.* **2004**, *16*, 4556–4573.
[78] D. Thirion, C. Poriel, J. Rault-Berthelot, F. Barrière, O. Jeannin, *Chem. Eur. J.* **2010**, *16*, 13646–13658.
[79] G. Zhou, M. Baumgarten, K. Müllen, *J. Am. Chem. Soc.* **2007**, *129*, 12211–12221.
[80] S. E. Braslavsky, *Pure Appl. Chem.* **2007**, *79*, 293–465.
[81] H. Etori, X. L. Jin, T. Yasuda, S. Mataka, T. Tsutsui, *Synth. Met.* **2006**, *156*, 1090–1096.
[82] J. Salbeck, N. Yu, J. Bauer, F. Weissörtel, H. Bestgen, *Synth. Met.* **1997**, *91*, 209–215.
[83] A. Iida, S. Yamaguchi, *Chem. Commun.* **2009**, 3002–3004.
[84] T. Qi, Y. Liu, W. Qiu, H. Zhang, X. Gao, Y. Liu, K. Lu, C. Du, G. Yu, D. Zhu, *J. Mater. Chem.* **2008**, *18*, 1131–1138.
[85] K. L. Chan, M. Sims, S. I. Pascu, M. Ariu, A. B. Holmes, D. D. C. Bradley, *Adv. Funct. Mater.* **2009**, *19*, 2147–2154.
[86] M. Leclerc, *J. Polym. Sci. Part A: Polym. Chem.* **2001**, *39*, 2867–2873.
[87] M. Sims, D. D. C. Bradley, M. Ariu, M. Koeberg, A. Asimakis, M. Grell, D. G. Lidzey, *Adv. Funct. Mater.* **2004**, *14*, 765–781.
[88] R. Abbel, M. Wolffs, R. A. A. Bovee, J. L. J. van Dongen, X. Lou, O. Henze, W. J. Feast, E. W. Meijer, A. P. H. J. Schenning, *Adv. Mater.* **2009**, *21*, 597–602.
[89] E. J. W. List, R. Guentner, P. Scanducci de Freitas, U. Scherf, *Adv. Mater.* **2002**, *14*, 374–378.
[90] M. A. Baldo, R. J. Holmes, S. R. Forrest, *Phys. Rev. B* **2002**, *66*, 035321.
[91] J.-W. Kang, D.-S. Lee, H.-D. Park, Y.-S. Park, J. W. Kim, W.-I. Jeong, K.-M. Yoo, K. Go, S.-H. Kim, J.-J. Kim, *J. Mater. Chem.* **2007**, *17*, 3714–3719.
[92] B. J. Chen, X. W. Sun, K. R. Sarma, *Mater. Sci. Eng. B* **2007**, *139*, 192–196.
[93] A. Altomare, M. C. Burla, M. Camalli, G. L. Cascarano, C. Giacovazzo, A. Guagliardi, A. G. G. Moliterni, G. Polidori, R. Spagna, *J. Appl. Crystallogr.* **1999**, *32*, 115–119.
[94] G. M. Sheldrick, *Acta Crystallogr. Sect. A* **2008**, *64*, 112–122.
[95] L. Farrugia, *J. Appl. Crystallogr.* **1999**, *32*, 837–838.

Received: March 15, 2011
Revised: June 16, 2011
Published online: September 27, 2011

